Synchronizing Torque Impacts on Rotor Speed in Power Systems

Mostafa Bakhtvar, Eknath Vittal, *Member, IEEE,* Kuan Zheng, and Andrew Keane, *Senior Member, IEEE*

***Abstract*—Renewables are increasingly replacing power from conventional generators. Renewable power injected through power electronic converters lacks the fundamental electric torque components. Electric torque components have an important role in determining the behavior of conventional machines in the network. The influence of this factor becomes more notable in power systems with reduced inertia. Hence, questions arise on, how can synchronizing torque basically contribute to the rotor speed deviation and eventually the system frequency and if there is a potential for using the steady state synchronizing torque coefficient (STC) to achieve acceptable frequency operating points. This paper calculates the steady state STC matrix by using the multi-machine Heffron-Philips model in conjunction with the network admitance matrix. Accordingly, it investigates the impact of the generator location and reactive power output on the STC matrix. It demonstrates how this impact manifests in the generator rotor speed deviation. Eventually, the significance of the STC from the system frequency perspective is assessed.**

***Index Terms*—operation, frequency, reactive power, synchronizing torque, wind generation, rate of change of frequency**

I. Introduction

ELECTRICAL power systems are designed on the basis of large centralized conventional synchronous generation units that rotate in synchronism with each other. Rotation of the shaft in synchronous generators, inherently, produces and injects electrical torque to the system. The active power injected by synchronous machines maintains synchronism and damps mechanical oscillations through the synchronizing and damping torque components of the electric torque, respectively.

There is an ever growing effort towards the reduction of emissions in power generation sector. Further addition of renewables to the power systems and the decommissioning of high polluting power plants e.g. coal plants in the US [1] are considered as approaches of interest. Consequently, renewable energy sources are replacing power from conventional synchronous units. Renewables often inject power to the network through power electronic converters resulting in decoupling of the mechanical input and the electrical output. Accordingly, the electrical torque component is absent from asynchrounous power injected into the network by renewables. This is a fundamental difference between conventional synchronous generation and renewable generation [2].

Originally, the abundance of synchronous inertia and electrical torque from synchronous generators together with their associated controls would allow for mitigation of large active and reactive power changes in the network. However, the increasing penetration of asynchronous generation raises apprehensions in this regard.

A combination of emulated inertial response from asynchronous resources, in particular wind generation [3]–[7], and governor response from remaining synchronous generators appears to be sufficient to meet reliability and reserve requirements in most systems [8], [9]. Additionally, it has been demonstrated that the design and implementation of power system stabilizers (PSS) on power electronic controlled devices [10]–[12] and more targeted control of reactive power [2], [13] can help damp mechanical oscillations between machines. However the provision of synchronizing torque depends on the presence of synchronous machines.

The synchronizing torque has a significant role in determining the initial rotor speed behavior of conventional generators following an event on the network. The immediate impact of synchronizing torque can be observed in two ways: first the initial angular deviation and second the instantaneous rate of change of rotor speed (ROCORS) following a major event in the network e.g. loss of generation. The machine rotor speed is tightly linked to the frequency throughout the system. It is vital to determine the contribution of synchronizing torque to the rotor speed deviation.

This paper calculates the steady state synchronizing torque coefficient (STC) matrix by modifying the multi-machine Heffron-Philips model given in [14]. It analyzes the steady state STC matrix in order to identify the effect of generator location and reactive power output on the elements of this matrix when active power output is fixed. It explores on how this effect manifests in the initial ROCORS of a generator for a power imbalance event elsewhere in the network. This interaction of generators translates to the rate of change of frequency (ROCOF) in the network. It is shown that for systems with reduced inertia and synchronizing torque, a ROCOF improvement can be realized using this characteristic. ROCOF has been identified as a bottleneck for high asynchronous generation penetration in power systems [15]. Monitoring the elements of the STC matrix enables achieving acceptable frequency operating points. The results from this

This work was conducted in the Electricity Research Centre, University College Dublin, Ireland, which is supported by the Electricity Research Centre's Industry Affiliates Programme (http://erc.ucd.ie/industry/). This material is based upon works supported by the Science Foundation Ireland, by funding M. Bakhtvar, under Grant No. SFI/09/SRC/E1780. The opinions, findings and conclusions or recommendations expressed in this material are those of the author(s) and do not necessarily reflect the views of the Science Foundation Ireland.

M. Bakhtvar (mostafa.bakhtvar@ucd.ie) and A. Keane (andrew.keane@ucd.ie) are with University College Dublin, Dublin, Ireland. E. Vittal (evittal@epri.com) is with Electric Power Reserch Institute, Palo Alto, CA, USA. K. Zheng (zhengk11@mails.tsinghua.edu.cn) is with Tsinghua University, Beijing, China.

paper provides foundation to help system operators establish strategies that benefit from the STC matrix characteristics in order to improve stability.

The paper will be divided as follows: Section II will describe the derivation of STC matrix from the multi-machine Heffron-Philips model and its implications on the generator rotor speed and system frequency. Section III will describe the test systems that the analysis is completed on. Section IV will provide a discussion of the results and finally Section V will conclude this paper.

II. SYNCHRONIZING TORQUE AND SYSTEM STABILITY

A. The synchronizing torque coefficient

Synchronizing torque is a component of the electrical torque produced by a synchronous generator. As defined by [16], synchronizing torque is "*... the most important component of the electrical torque. It is produced by the interaction of the stator windings with the fundamental component of the air gap flux. It is dependent upon the machine terminal voltage, the rotor angle, the machine reactances, and the so-called quadrature axis EMF.*" Using a single machine infinite bus model, in [17], the synchronizing torque of a synchronous machine is defined as a component of the electrical torque of the machine (1).

$$T_e(js) = \frac{\Delta T_e}{\Delta \delta} = T_s + jsT_d \tag{1}$$

where T_e is the electrical torque and T_s and T_d are the synchronizing torque and damping torque respectively.
Work in [18], expanded on this model and introduced the impact of excitation systems and voltage control. This is crucial, as the relationship and electrical connection between synchronous machines in a system are highly dependent on the voltage and angles between them. Reference [14] generalizes the single machine infinite bus Heffron-Phillips model for multi-machine systems, per Fig. 1, by referring all machines to a common D-Q reference frame and considering the change in the angle between each individual machine's d-q coordinates and the reference frame as state variables. Based on the origin, the change in the electric torque within this model can be divided in two parts per (2)

- changes due to variation in rotor angles, $\Delta\delta$
- changes due to variation in internal voltages, $\Delta E_q^{'}$

$$[\Delta T_e] = [K_1]\,[\Delta\delta] + [K_2]\left[\Delta E_q^{'}\right] \tag{2}$$

The variation in machine internal voltage may be written as a result of variation in field voltage, ΔE_{fd}, and rotor angles.

$$[J_1]\left[\Delta E_q^{'}\right] = [\Delta E_{FD}] - [K_4]\,[\Delta\delta] \tag{3}$$

The following steps are carried in order to derive an equation of the form $[\Delta Y] = [A]\,[\Delta X]$ for the change of electric torque-change of rotor angle characteristic based on the multi-machine Heffron-Philips given in [14].

For an excitation system per Fig. 2, substituting (17), from Appendix A, for $[\Delta V_t]$, the change in field voltage may be written as a function of variation in rotor angle and internal voltage

$$[\Delta E_{FD}] = -\,[J_2]\,[\Delta V_t] = -\,[J_2]\,[K_5]\,[\Delta\delta] - [J_2]\,[K_6]\left[\Delta E_q^{'}\right] \tag{4}$$

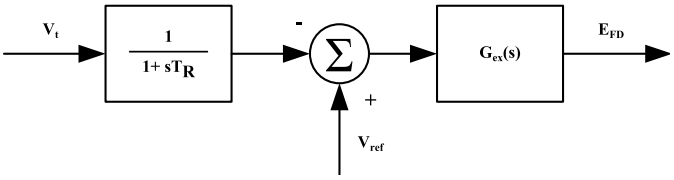

Fig. 2. A simplified excitation system

Substituting (4) in (3) yields

$$([J_1] + [J_2]\,[K_6])\left[\Delta E_q^{'}\right] = -([J_2]\,[K_5] + [K_4])\,[\Delta\delta] \tag{5}$$

Rewriting for $[\Delta T_e]$ using (2) and (5) gives

$$[\Delta T_e] = [\Pi]\,[\Delta\delta] \tag{6}$$

Where the $[\Pi]$ matrix is defined as a combination of $[K_1]$, $[K_2]$ and $[\Gamma]$ matrices.

$$[\Pi] = [K_1] + [K_2]\,[\Gamma] \tag{7}$$

$$[\Gamma] = -([J_1] + [J_2]\,[K_6])^{-1}([J_2]\,[K_5] + [K_4]) \tag{8}$$

The $[K_1]$ matrix gives the change in the electric torque for a change in the rotor angles when the internal voltage is constant. The $[K_2]$ matrix gives the change in the electric torque for a change in the internal voltage when the rotor angles are constant. The $[\Gamma]$ matrix gives the change in the internal voltage for a change in the rotor angles; this includes the effect of the interaction of exciters through $[J_2]$, $[K_5]$ and $[K_6]$ matrices.

The resultant matrix, $[\Pi]$, is an $n \times n$ non-sparse and non-symmetrical matrix per:

$$\Pi = \begin{bmatrix} \Pi_{1,1} & \Pi_{1,2} & \cdots & \Pi_{1,n} \\ \Pi_{2,1} & \Pi_{2,2} & \cdots & \Pi_{2,n} \\ \vdots & \vdots & \ddots & \vdots \\ \Pi_{n,1} & \Pi_{n,2} & \cdots & \Pi_{n,n} \end{bmatrix}$$

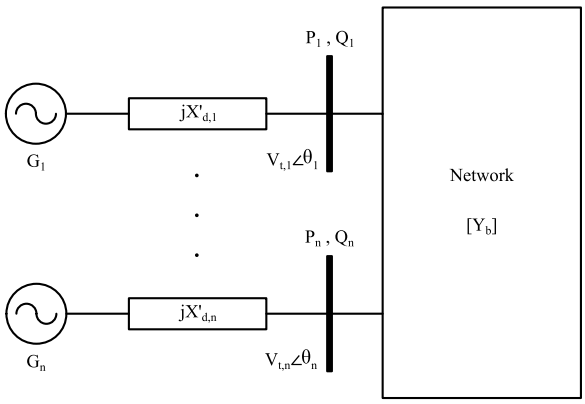

Fig. 1. Diagram representing the connection of synchronous generators to the network.

Where n is the number of generators. The $[\Pi]$ matrix gives the change in the electric torque for a change in the rotor angles; this is similar to the electric torque coefficient in a single machine Heffron-Philips model. However, the multi-machine extension depicts the interaction of the machines in the network.

In steady state the oscillation frequency, s, is equal to zero (no damping torque component in steady state), therefore:

$$\mathrm{Im}\left\{\Pi_{i,j}\right\} = 0 \qquad i,j = 1,2,\cdots,n$$

As such, the steady state STC components can be derived from the $[\Pi]$ matrix. According to equation (6), the change in the electric torque in each machine can be defined as

$$\Delta T_{e,i} = \sum_{j=1}^{G} \Pi_{i,j} \Delta\delta_j \tag{9}$$

Where $\Pi_{i,j}$ are elements of $[\Pi]$ matrix. It is seen using these elements, the change in the electric torque in each machine may be defined as a function of change in the rotor angle of all machines across the network. The elements in the $[\Pi]$ matrix can be separated into two groups

- diagonal elements, $\Pi_{i,i}$: The diagonal elements of $[\Pi]$ represent the total contribution of synchronizing torque from a machine to the network.
- off-diagonal elements, $\Pi_{i,j} \quad i \neq j$: The off diagonal elements of $[\Pi]$ represent the interaction between the machines.

A summary of the multi-machine Heffron-Phillips coefficients and $[J_1]$ and $[J_2]$ matrices definition can be found in Appendix A. The detailed model is available from [14].

The network admitance matrix and a common reference frame are used to calculate each of the *K* coefficient matrices and $[\Pi]$. Thus, the STC of the generator depends on two important factors. First, the location of the generator in the system which is defined by the respective elements in the reduced admitance matrix. Second, the contribution of reactive power (Q) from the generator which impacts the terminal voltage of the generator, V_t. Depending on the network conditions the elements in $[\Pi]$ can range from positive or negative. For the purpose of this paper i.e. characterizing the ROCORS-Q features of machines based on steady state, the effect of exciter was removed from the $[\Pi]$ matrix by letting $G_e x = 0$. This is reasonable due to the inherent delay in the main exciter field regardless of the regulator speed [16], [19] and that the parameter of interest is the initial ROCORS. Although it is not uncommon to model generators as a transient internal voltage $E^{'}$ behind transient reactance $X_d^{'}$ for first swing stability analysis [20]–[22], but the inclusion of the exciter and governor models is required for detailed analysis and multiswing studies [16], [23]. Thus, this assumption may not be valid for transient stability analysis, however, it is clarified that such an analysis is not the focus of this paper.

Further, it is emphasized that the removal of the effect of exciters is only associated with the multi-machine Heffron-Philips model employed for the calculation of the STC matrix (based on the steady state parameters). The time domain simulation presented in the following sections is done separately using the complete dynamic representation of the machines that may also be used for transient stability studies; this includes generator, exciter, power system stabilizer and governor models.

B. Impact on Frequency Response

The balance between mechanical power input and electrical power output is the fundamental relationship that governs power system stability. In modern power systems, the presence of control systems, particularly governors has reduced the dependence on the synchronizing torque contribution of machines. Following a generation/load imbalance the system will respond across three distinct time frames [16].

- *Electrical distance Effect ($t=0^+$)*: The transient period immediately following the event. The response in this time frame is associated with the electrical distance between generators.
- *Inertial Response ($0^+<t<t_g$)*: The period following the initial transient, when stored kinetic energy in the generators is released.
- *Governor Response ($t \geq t_g$)*: The time at which the governor control action of the generators takes over.

Inertial response and governor response are mechanical contributions of generators in response to the generation/load imbalance. The release of kinetic energy from the rotating mass of the synchronous generator arrests the fall of frequency and is the contribution of the inertial response. However, the benefits and impact of synchronizing torque are present only immediately following the generation/load imbalance and can be observed during the electrical distance effect. At t = 0^+, injection of active and reactive power will arrest the rate of rotor speed deviation, acceleration or deceleration, and the resulting deviation in the rotor angle of the generator. This phenomenon counters the rate of change of frequency at the generator bus. This electrical response is different from the mechanical response due to machine inertia. Often, the synchronizing power coefficient is used to describe the active power response of generators during this time period [16]. As this paper demonstrates, the change in the STC reveals the interaction of the machines in the power system and defines how a machine responds from both an active and reactive power perspective during the transient. The swing equation for the torque balance in the system defines this relationship as a function of the angular acceleration and the masses present in the system and is given in (10).

$$\frac{2H}{\omega_R}\frac{d^2\delta}{dt^2} = T_m - T_e \tag{10}$$

In (10), it is shown how the changes in the power balance are transferred to the rotor speed (frequency), ω, of machines in the system. The change in generator rotor speed will also be represented in the change in the angular position (δ) of the machines in the system. The response of the generator rotor speed will be dictated by the impact the change in electrical power and torque will have on the swing equation across the varying time-frames of response. The electrical distance effect,

as discussed earlier, occurs before the mechanical components of the power system respond, therefore the instantaneous changes from the losses of any T_{m_i} and T_{e_i} and the resulting response from T_{e_k}, where *i* and *k* are units across the system, will be represented in the acceleration of the angle, $\frac{d^2\delta}{dt^2}$. Since this is an exclusively electrical response, the machine angular speed is initially impacted by the presence of synchronizing torque. As such, this paper will examine the ROCORS at each generator. ROCORS is defined as the largest (absolute) rate of change of generator rotor speed in the first swing following a loss of generation event.

The analysis work is completed on the New England 39 bus test system to evaluate and assess the impact of reactive power on the STC in a non-diverse system. The results are verified by performing the study on a real world diverse system, the Irish 2020 network. The next section will describe these systems in detail.

III. Test System

A. New England 39 Bus

The modified New England 39 bus test system [24] was used to assess the impact of synchronizing torque on the power system. This system consisted of 10 synchronous units totaling 5000 MW supplying a system with a demand of 4965 MW and 1148 MVAr. The generators were modeled as identical units with round rotor generator models (GENROU), exciters (ESAC4A), governors (GAST) and stabilizers (PSS2A) [25]. The generators were set to control their terminal bus voltage to 1.0 pu. The active and reactive capabilities of each machine were the same along with the dynamic model used to represent the machine in the time domain. This was done in order to achieve non-diverse system where a comparison between all of the machines would only be influenced by the characteristics of the system. It is therefore possible to assess the impact that network topology and reactive power contribution have on the elements of the STC matrix. A network diagram of the New England test system can be seen in Fig. 3.

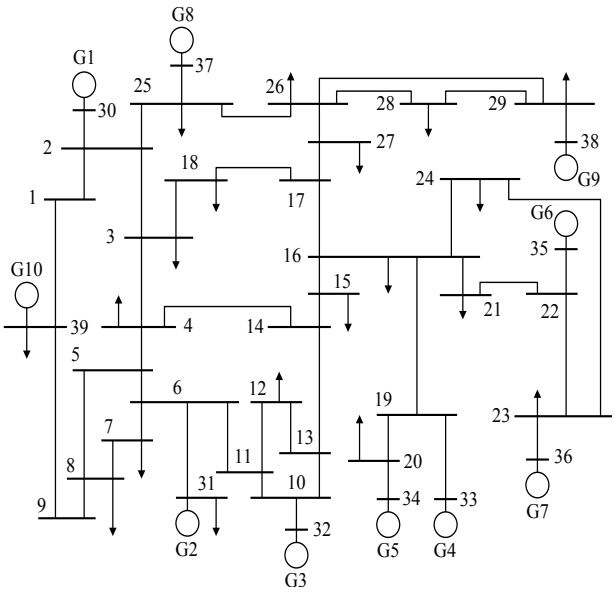

Fig. 3. Single line diagram of the New England 39 bus test system

B. All-Island Ireland 2020

In order to evaluate the applicability of the results, the all-island 2020 Irish transmission network was used [26]. This model provides for an analysis of a diverse system, where the generating units are unique and represent a real-life power system. Working from [26], an appropriate unit commitment and dispatch as well as an expected loading scenario were established for the 2020 system. The models of the synchronous generators were all generic models representative of the actual machines in the network, while the wind farms were modeled as aggregated models according to the type of farm [25]. The total generation in the system was 7274 MW, with 2339 MW and 748 MW being provided by wind generation and imports, respectively, i.e. 42% instantaneous penetration of non-synchronous generation in the system.

All simulations were completed in the DSATools software platform [27], with a 0.01 second time step. Python (NumPy) was used to calculate the parameters of the STC matrix. In each case a power flow case with the desired load and generation outputs was solved and used to initialize a time domain simulation. Based on the initial conditions and states of the generators in the time domain simulations, the necessary outputs were used to calculate the parameters described previously and the STC matrix in (7), prior to the contingency event. The generator rotor speed and system frequency are determined from the completed results of the time-domain simulation.

IV. Results and Discussion

A. Results on the New England 39 Bus Test System

The New England test system was used to establish the impacts of the STC.

1) Generator Location Effect:

The determined values for $\Pi_{i,i}$ can be seen in Table I.

TABLE I
Synchronizing torque coefficients at steady state for the New England test system

Generator	$\Pi_{i,i}$ (pu)
G1	0.28
G2	1.03
G3	0.97
G4	0.40
G5	0.15
G6	0.64
G7	0.01
G8	-0.38
G9	-1.21
G10	1.36

It is established that the values of the diagonal (and off diagonal) elements of the STC matrix are driven primarily by the topology of the network. This is particularly significant since in this test system the generators are all modeled identically.

This demonstrates that the level of the elements of the STC matrix varies based on the location of the generators and their reactive power outputs. There is up to 2.57 pu difference in $\Pi_{i,i}$. This difference is driven entirely by the reactive power and network topology.

2) Generator Reactive Power Output Effect:

To further demonstrate the effect of reactive power on the elements of the STC matrix, a generator was selected, in this case the generator at bus 35, G6, and the reactive power level of the generator was varied. The resulting impacts on the total synchronizing torque contribution (diagonal element of STC matrix) and the terminal voltage of the generator was observed and are presented in Table II.

TABLE II
SYNCHRONIZING TORQUE COEFFICIENT AND TERMINAL VOLTAGE AT VARYING REACTIVE POWER OUTPUTS OF G6

Reactive Power Output (MVAr)	**Terminal Voltage (pu)**	$\Pi_{6,6}$ **(pu)**
300	1.0564	2.257
250	1.0415	1.833
200	1.0261	1.391
150	1.0103	0.936
100	0.9939	0.459
50	0.977	-0.036
0	0.9593	-0.557
-50	0.941	-1.099
-100	0.9219	-1.668
-150	0.9019	-2.267
-200	*0.8809*	*-2.901*
-250	*0.8584*	*-3.586*

In Table II, the reactive power range of the generator is varied in 50 MVAr increments from -250 MVAr to 300 MVAr. The last two entries in the table (-250 and -200 MVAr) are italicized since the resulting terminal voltage values fall outside of standard operating conditions. They are included only to show the general pattern and progression in the STC elements. It can been seen that with the decrease in reactive power output, $\Pi_{6,6}$ became smaller. A full STC matrix when reactive power output of G6 is equal to -100 MVAr is given in Appendix B.

3) Effect on ROCORS:

To further examine the impact of the STC a contingency analysis was performed. For each reactive power setpoint, the generator at bus 36, G7, was tripped and the resulting impact on the ROCORS of G6 was observed. The ROCORS and corresponding diagonal ($\Pi_{6,6}$, $\Pi_{7,7}$) and off-diagonal ($\Pi_{6,7}$ and $\Pi_{7,6}$) elements of the STC matrix at each reactive power setpoint can be found in Fig. 4.

It can be seen that the ROCORS at G6 is sensitive to its reactive power output. As the reactive power output of the machine increased, the ROCORS of the machine decreased (faster ROCORS) in the transient following the contingency event. From (10) this indicates that immediately following the loss of G7 contingency the difference between T_m and T_e is greater as the reactive power output of G6 increases and as a result, the ROCORS of the generator is faster. The evolution of total STC contribution from G6, $\Pi_{6,6}$, through th reactive power setpoints shows a pattern in the opposite direction of the generator ROCORS characteristic. It is noted that with the increase of the reactive power set point, the interaction STC of G6 with respect to G7, $\Pi_{6,7}$, increased. In contrary, the opposite off-diagonal STC, that is G7 with respect to G6 ($\Pi_{7,6}$) decreased. This indicates that the sensitivity of the generators of interest, with respect to each other, can be altered solely by varying the reactive power of G6.

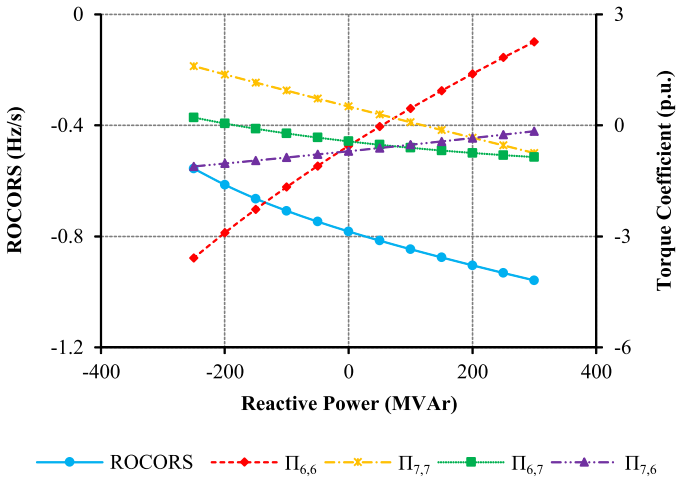

Fig. 4. Rate of change of rotor speed of G6 for the loss of G7 event and the respective synchronizing torque coefficient matrix elements against reactive power output of G6

Fig. 5 illustrates the pattern of the interaction STCs of G6 and G7, $\Pi_{6,7}$ and $\Pi_{7,6}$, against the G6 machine loading. The diagonal elements of the STC matrix, $\Pi_{6,6}$ and $\Pi_{7,7}$, are also shown in this figure. An intriguing feature of the shown characteristics is their correlation with the G6 MVA loading.

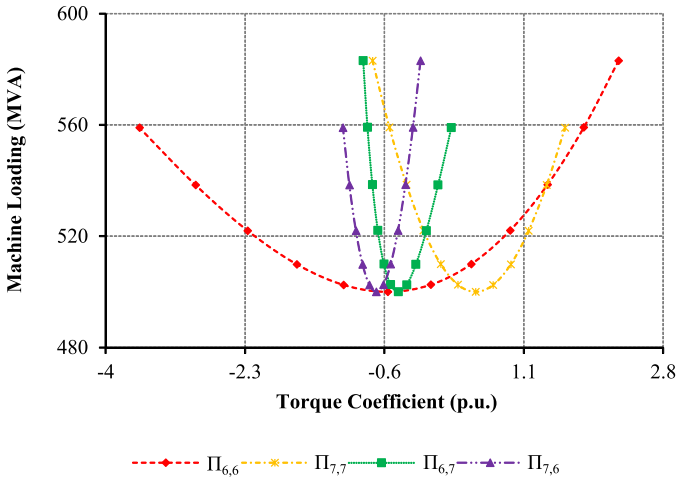

Fig. 5. Synchronizing torque coefficient elements for G6 and G7 over G6 machine loading

The effect of the interaction of G6 and G7 on the ROCORS of G6 is evaluated by calculating the ratio of the corresponding interaction factors i.e. $\Pi_{7,6}/\Pi_{6,7}$. It is anticipated that for the cases which both of the off-diagonal STC elements have sim-

ilar signs (same direction), faster ROCORS occur when ratio is zero. Vice versa, for cases that STC elements have different signs (opposite direction) slower ROCORS are expected when ratio is close to zero. This is logical as high sensitivity in the same direction results in a larger speed drop in the rotor of the machine of interest. Fig. 6 shows the explained aspect in the test system. It can be seen that significantly large ROCORS occurs when $\Pi_{7,6}/\Pi_{6,7}$ approaches zero in the positive side of the diagram.

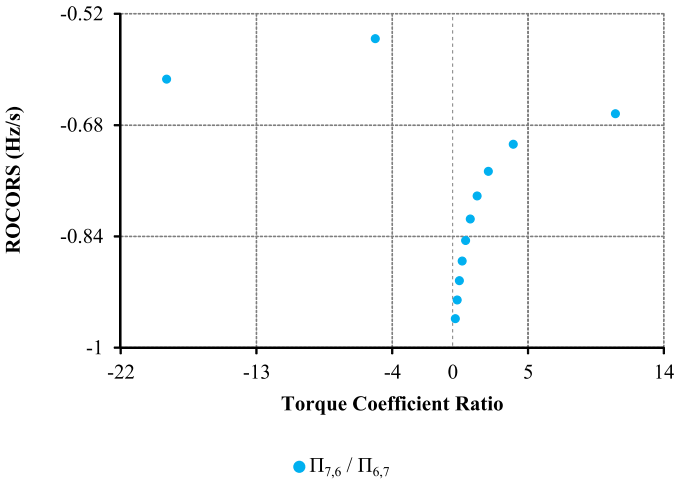

Fig. 6. Rate of change of rotor speed of G6 for loss of G7 event against the ratio of off-diagonal synchronizing torque coefficient elements

4) Rotor Speed Nadir Progression:

If the nadir of the machine is observed, it can be seen that it is closely correlated with the reactive power output of the machine. Fig. 7 shows the nadir of G6, for the varying reactive power output, for the loss of G7 event. It is observed that the rotor speed nadir of the generator improves as the reactive power output of the machine increases. The improvement slows down as the machine crosses from leading (inductive) to lagging (capacitive), the nadir begins to decrease slightly as the MVA loading of the machine increases. Recalling from Fig. 4, the faster ROCORS occurred when the machine injected reactive power in the network. As such, it is emphasized that realizing both optimum rotor speed nadir and ROCORS through reactive power may not necessarily align with each other.

5) System Perspective:

In order to demonstrate the significance of the synchronizing torque in a system with integrated wind (reduced synchronizing torque as well as inertia), the synchronous units, G3 and G9, were replaced by equivalent size (and output) wind farms. The wind farms were modeled as aggregated 1.5MW wind turbines equipped with emulated inertia [28]. The recommended parameters by [28] were used for this purpose. These parameters are reported to provide acceptable response from the wind farm in [29]. The trip of G7 event was considered and the reactive power output of G6 was varied while the remaining generators' reactive power output were used to control voltage at their terminals to 1 p.u.. The synchronizing torque contribution of G7 to the system as well as the ROCOF at the center of inertia is given in Table III.

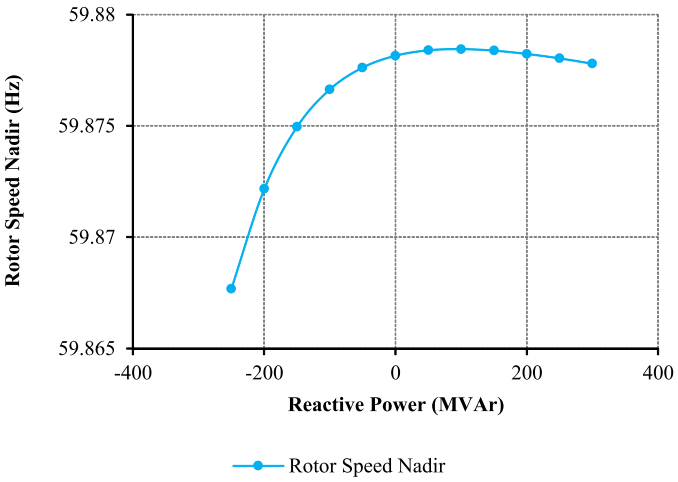

Fig. 7. G6 rotor speed nadir for loss of G7 event against G6 reactive power output

TABLE III
SYNCHRONIZING TORQUE CONTRIBUTION FOR G7 AT VARIOUS G6 REACTIVE POWER OUTPUTS

Reactive Power Output (MVAr)	Π_{77} (p.u.)	ROCOF (Hz/s)
300	-0.734	-0.488
200	-0.319	-0.471
100	0.101	-0.454
0	0.530	-0.434
-100	0.961	-0.413
-250	1.629	-0.375

It is noticed that the more positive (larger) $\Pi_{7,7}$, the slower the ROCOF is. Indeed, higher injection of synchronizing torque (loss of higher sensitivity in the speed drop direction) is expected to result in slower ROCOF.

The frequency trend at the center of inertia is illustrated in Fig. 8. When G6's reactive power set point is equal to 100 MVAr, the frequency drop in the system cannot be arrested. This condition worsens for higher reactive power set points.

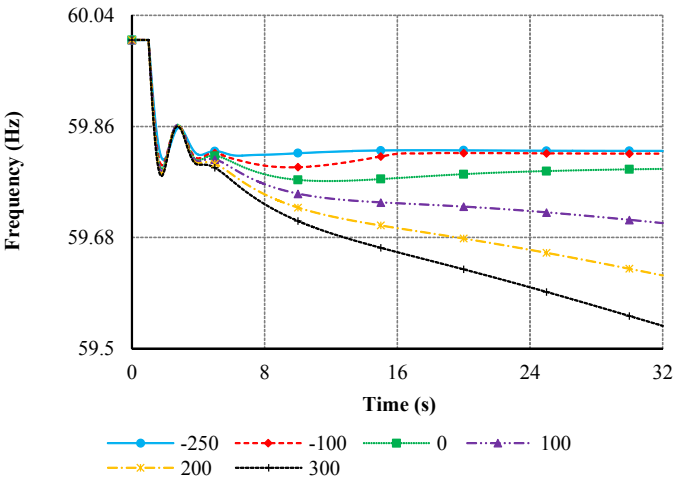

Fig. 8. Frequency trace at center of the inertia for the loss of G7 event at various G6 reactive power outputs

B. Results on the All-Island Irish 2020 Test System

The validity of the established characteristics for diverse systems is investigated using the Irish power system model. Generators G1 and G2 are two generators with unique dynamic models. The inertia of G1 is higher than G2. Both of these generators produce 400 MW. The reactive power of these generators is varied in 50 MVAr steps.

1) Interaction of Proximate Generators:

At each reactive power setting, time domain analysis is carried for the trip of G1 and G2, individually. The generators' rotor speed is recorded throughout the system. The aim is to assess the impact of the reactive power output setting of generators within close distance on each others ROCORS when one generator is tripped. Fig. 9 shows heat maps for ROCORS at each reactive power setting of generators G1 and G2 when the other generator is tripped. It can be seen that the ROCORS range is $0.37 - 0.86$ and $0.36 - 0.75$ Hz/s for G1 and G2, respectively. This large range was obtained solely by varying the reactive power power setting of these generators. This emphasizes the impact shown in section IV-A. Also, it is noted that the reactive power setting leading to the slowest ROCORS performance of these generators do not overlap. G1 has the slowest ROCORS behavior in the region in the heat map that G2 shows lower ROCORS (faster) values.

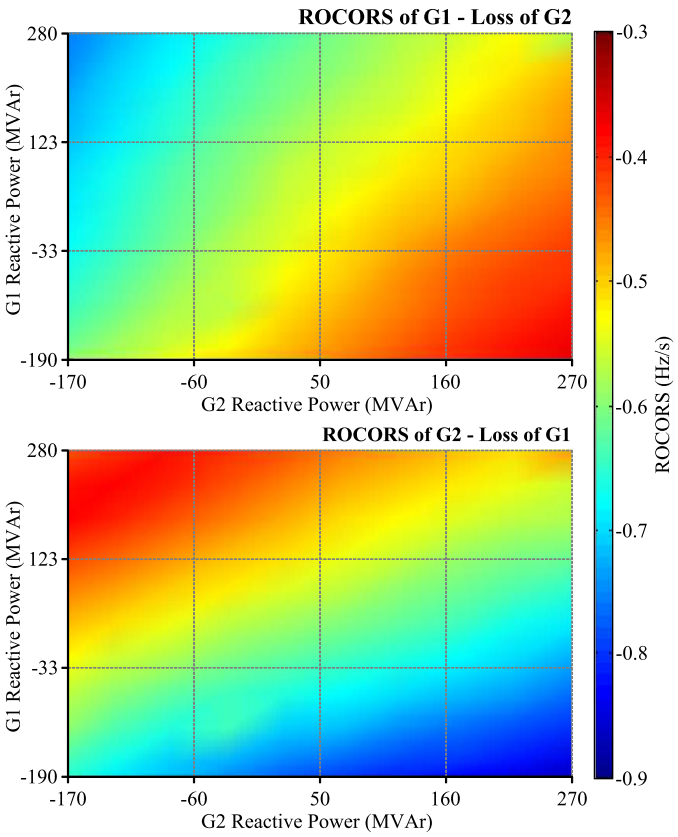

Fig. 9. Rate of change of rotor speed versus reactive power setting for G1 and G2 in the Irish network

2) Operating Point Adjustment:

In order to demonstrate the connection of this phenomenon with the STC, the ratio of the corresponding off diagonal elements of the Π matrix i.e. $\frac{\Pi_{2,1}}{\Pi_{1,2}}$ is calculated at each of the reactive power output settings shown in Fig. 9. Fig. 10 illustrates this ratio against the ROCORS at generators G1 and G2 when the other generator is tripped. It can be seen that in both trends, the high (positive) ratio of $\frac{\Pi_{j,i}}{\Pi_{i,j}}$ is equivalent to slower ROCORS. Where i is the generator under study and j is the generator tripped. Accordingly, the trends shown in Fig. 10 go in opposite directions. Further, it is noted that the best behavior of these generators occurred when $\frac{\Pi_{j,i}}{\Pi_{i,j}} = 1$. These are inline with the heat maps illustrated in Fig. 9.

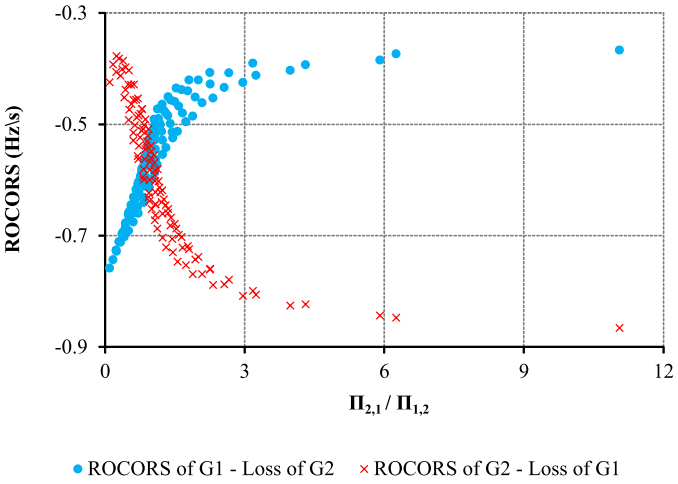

Fig. 10. Rate of change of rotor speed over the ratio of the off-diagonal synchronizing torque coefficient matrix elements for G1 and G2 in the Irish network

3) System Perspective:

Fig. 11 looks at the phenomenon from the point of view of the frequency at the system center of inertia. This figure plots the ROCOF at the center of inertia against the synchronizing torque contribution, $\Pi_{j,j}$ (where j is the generator tripped). Similar to the behavior seen in section IV-A, it can be seen that in general higher (more positive) values of synchronizing torque are more favorable from the ROCOF perspective. The impact on ROCOF shown in this figure is significant and valuable for secure operation of the power system under low inertia.

V. Conclusion

The Heffron-Philips model was modified to derive the synchronizing torque coefficient (STC) matrix. The impact of network topology and generator reactive power output on STC matrix elements was demonstrated. It was seen that the rate of change of rotor speed (ROCORS) of generators is sensitive to their reactive power output. The correlation of the STC matrix elements with generators' ROCORS was shown. The presented methodology enables identification of critical machines in order to limit their ROCORS based on the STC matrix. The replacement of synchronous generators by wind farms results in a reduced synchronizing torque and inertia case. The importance of the synchronizing torque from the system frequency perspective was discussed and presented for this case. It was established that the reactive power output of generators can be utilized to manage the steady state STC of

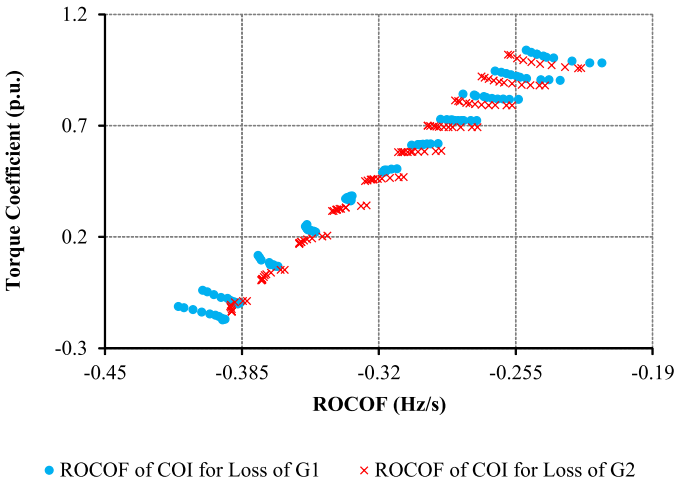

Fig. 11. Rate of change of frequency at the center of inertia over synchronizing torque contribution of G1 and G2 in the Irish network

conventional units, ROCORS and ultimately the system rate of change of frequency (ROCOF). This characteristic provides valuable indication for secure power system operation from the frequency perspective. The applicability of the results were verified on a diverse system with large penetration of non-synchronous power. It was seen that an optimum solution from one generator perspective may not be favored from the perspective of other generators in the network. Using the STC matrix, there is a potential for adjusting generator voltage set points such that not only they support voltage in the network but also mitigate frequency and rotor angle excursion. Many systems already operate with minimum inertia standards, accordingly, as the penetration of renewables increase, monitoring the STC matrix elements will be beneficial in controlling the frequency behavior.

Appendix A
Multi-Machine Heffron-Phillips Model

$$[K_{1,ij}] = (E^{'}_{q,i} + (X_{q,i} - X^{'}_{d,i}))F_{q,ij} + ((X_{q,i} - X^{'}_{d,i})I_{q,i})F_{d,ij} \tag{11}$$

$$[K_{2,ij}] = \begin{cases} I_{q,i} + (E^{'}_{q,i} + (X_{q,i} - X^{'}_{d,i})I_{d,i})Y_{q,ii} + (X_{q,i} - X^{'}_{d,i})Y_{d,ii} & i = j \\ (E^{'}_{q,i} + (X_{q,i} - X^{'}_{d,i}))F_{q,ij} + ((X_{q,i} - X^{'}_{d,i})I_{q,i})Y_{d,ij} & i \neq j \end{cases} \tag{12}$$

$$[K_{3,ij}] = \begin{cases} (1 - (X_{d,i} - X^{'}_{d,i})Y_{d,ii})^{-1} & i = j \\ ((X_{d,i} - X^{'}_{d,i})Y_{d,ii})^{-1} & i \neq j \end{cases} \tag{13}$$

$$[K_{4,ij}] = (X_{d,i} - X^{'}_{d,i})F_{d,ij} \tag{14}$$

$$[K_{5,ij}] = \frac{V_{d,i}X_{q,i}F_{q,ij} - V_{q,i}X^{'}_{d,i}F_{d,ij}}{V_i} \tag{15}$$

$$[K_{6,ij}] = \begin{cases} \frac{V_{d,i}X_{q,i}Y_{q,ii} + V_{q,i}(1 - X^{'}_{d,i}Y_{d,ii})}{V_i} & i = j \\ \frac{V_{d,i}X_{q,i}Y_{q,ij} - V_{q,i}X^{'}_{d,i}Y_{d,ij}}{V_i} & i \neq j \end{cases} \tag{16}$$

$$[\Delta V_t] = [K_5][\Delta\delta] + [K_6]\left[\Delta E^{'}_q\right] \tag{17}$$

$$[J_{1,ij}] = \begin{cases} \frac{1}{K_{3,ii}} + sT^{'}_{do,i} & i = j \\ \frac{1}{K_{3,ij}} & i \neq j \end{cases} \tag{18}$$

$$[J_{2,ij}] = [G_{ex}][G_{tr}] = \begin{cases} \frac{G_{ex,i}}{1+sT_{R,i}} & i = j \\ 0 & i \neq j \end{cases} \tag{19}$$

Appendix B
A Sample [Π] Matrix

[Π] matrix for $Q_6 = -100$ MVAr operating point

$$\Pi = \begin{bmatrix} 0.45 & 0.06 & 0.04 & 0.03 & 0.04 & -0.23 & 0.03 & -0.42 & -0.19 & 0.18 \\ -0.15 & 1.16 & -0.37 & -0.05 & -0.04 & -0.30 & -0.05 & -0.19 & -0.10 & 0.09 \\ -0.14 & -0.33 & 1.14 & -0.07 & -0.06 & -0.32 & -0.07 & -0.18 & -0.10 & 0.13 \\ 0.01 & 0.12 & 0.08 & 0.78 & -0.62 & -0.43 & -0.16 & -0.06 & -0.04 & 0.32 \\ 0.06 & 0.17 & 0.13 & -0.56 & 0.31 & -0.37 & -0.09 & 0.00 & 0.02 & 0.34 \\ 0.23 & 0.33 & 0.30 & 0.11 & 0.12 & -1.67 & -0.21 & 0.16 & 0.19 & 0.45 \\ -0.02 & 0.10 & 0.05 & -0.20 & -0.17 & -0.87 & 0.94 & -0.09 & -0.07 & 0.32 \\ -0.27 & 0.15 & 0.13 & 0.10 & 0.11 & -0.15 & 0.11 & -0.26 & -0.17 & 0.25 \\ -0.01 & 0.26 & 0.23 & 0.15 & 0.16 & -0.11 & 0.16 & -0.13 & -1.08 & 0.37 \\ -0.30 & -0.18 & -0.16 & -0.03 & -0.02 & -0.27 & -0.03 & -0.31 & -0.16 & 1.46 \end{bmatrix}$$

Acknowledgement

The authors would like to acknowledge Michael Power and EirGrid Plc. for their insightful advice and assistance with this paper.

References

[1] J. M. Melillo, T. T. Richmond, and G. Yohe, "Climate change impacts in the united states," *Third National Climate Assessment*, 2014.
[2] E. Vittal, M. O'Malley, and A. Keane, "Rotor angle stability with high penetrations of wind generation," *Power Systems, IEEE Transactions on*, vol. 27, no. 1, pp. 353–362, Feb 2012.
[3] G. Ramtharan, J. Ekanayake, and N. Jenkins, "Frequency support from doubly fed induction generator wind turbines," *Renewable Power Generation, IET*, vol. 1, no. 1, pp. 3–9, March 2007.
[4] J. Morren, S. de Haan, W. Kling, and J. Ferreira, "Wind turbines emulating inertia and supporting primary frequency control," *Power Systems, IEEE Transactions on*, vol. 21, no. 1, pp. 433–434, Feb 2006.
[5] G. Lalor, A. Mullane, and M. O'Malley, "Frequency control and wind turbine technologies," *Power Systems, IEEE Transactions on*, vol. 20, no. 4, pp. 1905–1913, Nov 2005.
[6] D. Gautam, L. Goel, R. Ayyanar, V. Vittal, and T. Harbour, "Control strategy to mitigate the impact of reduced inertia due to doubly fed induction generators on large power systems," *Power Systems, IEEE Transactions on*, vol. 26, no. 1, pp. 214–224, Feb 2011.
[7] M. Kayikci and J. Milanovic, "Dynamic contribution of dfig-based wind plants to system frequency disturbances," *Power Systems, IEEE Transactions on*, vol. 24, no. 2, pp. 859–867, May 2009.
[8] P. Kundur, N. J. Balu, and M. G. Lauby, *Power system stability and control*. McGraw-hill New York, 1994, vol. 7.
[9] P. Kundur, J. Paserba, V. Ajjarapu, G. Andersson, A. Bose, C. Canizares, N. Hatziargyriou, D. Hill, A. Stankovic, C. Taylor, T. Van Cutsem, and V. Vittal, "Definition and classification of power system stability ieee/cigre joint task force on stability terms and definitions," *Power Systems, IEEE Transactions on*, vol. 19, no. 3, pp. 1387–1401, Aug 2004.
[10] F. Hughes, O. Anaya-Lara, N. Jenkins, and G. Strbac, "A power system stabilizer for dfig-based wind generation," *Power Systems, IEEE Transactions on*, vol. 21, no. 2, pp. 763–772, May 2006.
[11] G. Tsourakis, B. Nomikos, and C. Vournas, "Contribution of doubly fed wind generators to oscillation damping," *Energy Conversion, IEEE Transactions on*, vol. 24, no. 3, pp. 783–791, Sept 2009.
[12] A. Mendonca and J. P. Lopes, "Robust tuning of power system stabilisers to install in wind energy conversion systems," *IET Renewable Power Generation*, vol. 3, no. 4, pp. 465–475, 2009.
[13] C. W. Taylor, *Power system voltage stability*. McGraw-Hill, 1994.
[14] M. El-Sharkawi, "Estimation of dynamic equivalents of external electric power systems," Ph.D. dissertation, Department of Engineering, Universtiy of British Columbia, 1980.

[15] "All island TSO facilitation of renewables studies," EirGrid Plc., Tech. Rep., 2009.
[16] P. M. Anderson and A. A. Fouad, *Power system control and stability*. John Wiley & Sons, 2008.
[17] R. Shepherd, "Synchronizing and damping torque coefficients of synchronous machines," *Power Apparatus and Systems, Part III. Transactions of the American Institute of Electrical Engineers*, vol. 80, no. 3, pp. 180–189, April 1961.
[18] F. Demello and C. Concordia, "Concepts of synchronous machine stability as affected by excitation control," *Power Apparatus and Systems, IEEE Transactions on*, vol. PAS-88, no. 4, pp. 316–329, April 1969.
[19] E. Kimbark, *Power System Stability, Volume III: Synchronous Machines*, ser. Power System Stability. John Wiley & Sons, 1995.
[20] S. Ramar and S. Kuruseelan, *Power system analysis*. PHI Learning, 2013.
[21] P. Murthy, *Power System Analysis*. BS Publications, 2007. [Online]. Available: https://books.google.ie/books?id=V-qIoAEACAAJ
[22] L. Singh, *Advanced Power System Analysis and Dynamics*. New Age International, 2006. [Online]. Available: https://books.google.co.uk/books?id=vECbHnSx_wcC
[23] P. G. Brown, F. P. Demello, E. H. Lenfest, and R. J. Mills, "Effects of excitation, turbine energy control, and transmission on transient stability," *IEEE Transactions on Power Apparatus and Systems*, vol. PAS-89, no. 6, pp. 1247–1252, July 1970.
[24] M. A. Pai, *Computer techniques in power system analysis*. Tata McGraw-Hill Publishing Company, 1979.
[25] *PSSE Program Operations Model Library*, Siemens Energy , Inc., Siemens Power Technologies International, October 2010.
[26] "All island transmission forecast statement," EirGrid Plc., Tech. Rep., May 2010.
[27] *DSATools User Manual*, Powertech Labs Inc., Surrey British Columbia, Canada, 2007.
[28] Y. Kazachkov, P. Keung, and K. Patil, *PSSE Wind Modeling Package for GE 1.5/3.6/2.5 MW Wind Turbines User Guide*, Siemens, June 2009.
[29] M. Seyedi and M. Bollen, "The utilization of synthetic inertia from wind farms and its impact on existing speed governors and system performance," Elforsk, Tech. Rep., January 2013.

Mostafa Bakhtvar (S'12) received his Ph.D. in electrical engineering and M.E. in energy systems engineering from University College Dublin, Ireland, in 2016 and 2012, respectively; he completed the B.Sc. degree in electric-power engineering at IAU-Saveh, Iran, in 2010. He is currently a senior researcher with the School of Electrical and Electronic Engineering, University College Dublin. His research interests include, distribution and transmission system planning, operation, optimization and stability.

Eknath Vittal (S'07-M'11) received his Ph.D. from University College Dublin in 2011, he completed his M.Sc. and B.Sc. from Iowa State University and the University of Illinois Urbana-Champaign respectively. He is currently a research engineer at the Electric Power Research Institute in Palo Alto, CA. His research focus is in the area of transient stability analysis and transmission system planning with changing generation resources.

Kuan Zheng received the B.Sc. degree in electrical engineering in 2011. She is currently pursuing the Ph.D. degree in the Department of Electrical Engineering, Tsinghua University, China. Her research interests include wind power integration and power system stability.

Andrew Keane (S'04-M'07-SM'14) received the Ph.D. degree in electrical engineering from University College Dublin, Ireland in 2007. He is an Associate Professor and Head of the School of Electrical and Electronic Engineering, University College Dublin. He is also Head of the Energy Institute at UCD. He has previously worked with ESB Networks, the Irish Distribution System Operator. His research interests include power systems planning and operation, distributed energy resources, and distribution networks.